
THE MODEL KNOWS WHICH TOKENS MATTER: AUTOMATIC TOKEN SELECTION VIA NOISE GATING

Landi He

Shenzhen University of Advanced Technology

Xiaoyu Yang

Shenzhen University of Advanced Technology

Lijian Xu *

Shenzhen University of Advanced Technology
xulijian@suat-sz.edu.cn

March 10, 2026

ABSTRACT

Visual tokens dominate inference cost in vision-language models (VLMs), yet many carry redundant information. Existing pruning methods alleviate this but typically rely on attention magnitude or similarity scores. We reformulate visual token pruning as capacity constrained communication: given a fixed budget K , the model must allocate limited bandwidth to maximally preserve visual information. We propose **AutoSelect**, which attaches a lightweight Scorer and Denoiser to a frozen VLM and trains with only the standard next token prediction loss, without auxiliary objectives or extra annotations. During training, a variance preserving noise gate modulates each token’s information flow according to its predicted importance so that gradients propagate through all tokens; a diagonal attention Denoiser then recovers the perturbed representations. At inference, only the Scorer and a hard top- K selection remain, adding negligible latency. On ten VLM benchmarks, AutoSelect retains 96.5% of full model accuracy while accelerating LLM prefill by $2.85\times$ with only 0.69 ms overhead, and transfers to different VLM backbones without architecture-specific tuning. Code is available at <https://github.com/MedHK23/AutoSelect>.

1 Introduction

Vision-language models (VLMs) that couple a pretrained visual encoder with a large language model (LLM) have become the prevailing paradigm for visual question answering, multimodal dialogue, and cross-modal reasoning. In the standard pipeline, patch or grid features from the encoder are projected into the LLM’s embedding space and typically prepended as visual tokens for autoregressive decoding, as seen in representative models like BLIP-2, InstructBLIP, and LLaVA [1, 2, 3]. However, as these models are increasingly applied to high-resolution images and multi-image or video scenarios, the resulting surge in visual tokens creates a severe computational bottleneck. Due to the quadratic scaling of self-attention with respect to sequence length, these abundant visual tokens quickly dominate both inference computation and memory.

Empirical studies reveal substantial redundancy among visual tokens. Attention distributions are typically highly concentrated, with only a small subset of tokens receiving significant attention while a large fraction exhibits near-zero attention across layers [4, 5]. Nevertheless, subsequent layers still allocate full self-attention computation to all tokens, including those with negligible contribution to the final prediction. These observations suggest that substantial computational redundancy exists in current VLM pipelines.

Existing pruning methods tackle this challenge from multiple directions, including inference-time token and key-value (KV) cache optimization [6], layer-wise budget search [7], and instruction-aware or cross-modal selection strategies [8, 9, 10]. While these approaches achieve useful speed–accuracy trade-offs, their selection criteria are

*Corresponding author

typically based on local proxy signals such as attention magnitude, similarity scores, or predefined pruning schedules. Consequently, pruning is primarily formulated as identifying and discarding “less important” tokens. This perspective overlooks a more fundamental question: given a fixed computational budget, how should representational capacity be globally allocated across visual tokens to maximize downstream reasoning performance?

We approach this problem by recasting visual token pruning as **capacity-constrained representation learning**. As illustrated in Figure 1, a pruning module sits between the visual encoder and the LLM. Existing methods treat this module as a hard filter that irreversibly discards tokens, whereas we model the same encoder–LLM interface as a bandwidth-limited channel in which a fixed token budget K constrains the total information capacity rather than the token count. During training, no tokens are removed; instead, the effective information throughput of each token is continuously modulated by its importance score, so that a budget of K tokens worth of capacity is allocated to the most informative content. Under this formulation, the objective shifts from identifying dispensable tokens to constructing a compact representation that maximizes useful information within the prescribed capacity.

We introduce two lightweight plug-in modules, a Scorer and Denoiser, while keeping the pretrained VLM entirely frozen. During training, no tokens are discarded; importance scores from the Scorer modulate information flow through a continuous bottleneck, attenuating low-scoring tokens under a fixed capacity constraint. This reformulates discrete pruning as a differentiable capacity allocation objective optimized end-to-end. A Denoiser then remaps noise-perturbed tokens back into the distribution expected by the frozen LLM, operating independently on each token to prevent information leakage. At inference, the continuous bottleneck is replaced by hard top- K selection: only the highest-scoring tokens are forwarded to the LLM, yielding computational savings without modifying the base architecture.

Our contributions are threefold:

- 1) We reformulate visual token pruning as *capacity-constrained representation learning*, modeling the visual encoder–LLM interface as a bandwidth-limited channel. The resulting framework is optimized with the standard next-token prediction loss as its sole training objective, without auxiliary losses, external annotations, or modifications to the base VLM.
- 2) We introduce a variance-preserving noise gate that replaces the binary keep-or-discard decision of conventional pruning with continuous per-token information capacity modulation. Paired with a Soft Top- K operator and temperature annealing, this mechanism provides full gradient flow during training while converging to hard Top- K selection at inference.
- 3) AutoSelect retains 96.5% of full-model performance at 88.9% pruning on LLaVA-1.5-7B with only 0.69 ms pruning module overhead, and generalizes consistently to the higher-resolution LLaVA-NEXT and the architecturally distinct Qwen2.5-VL.

2 Related Work

2.1 VLMs and Efficient Paradigms

Large vision-language models (VLMs) have rapidly progressed by coupling visual perception with the generative and reasoning capabilities of large language models (LLMs) [11, 12, 13, 14]. Most contemporary open VLMs adopt an “encode-and-project” paradigm, where image patches are encoded into visual tokens and mapped into the LLM token space via learned projectors, cross-attention, or query-based resamplers [3, 1, 15]. Instruction tuning and dialogue-style supervision further align these models to follow human prompts and generalize across vision-language tasks [3, 2]. Beyond encoder-based pipelines, EVE [16] explores encoder-free unified-decoder training to improve architectural flexibility and efficiency when mixing vision and language streams.

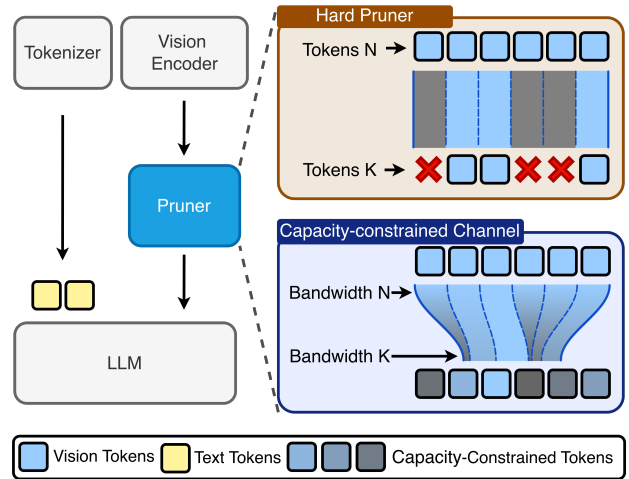


Figure 1: **Two views of visual token pruning.** (Top) Hard pruning directly discards a subset of tokens. (Bottom) Our capacity-constrained formulation retains all tokens but limits the total information throughput to the same budget through a bandwidth-limited channel.

As VLMs scale to richer visual inputs, including high-resolution images, arbitrary aspect ratios, multi-image interleaving, and video, the number of visual tokens increases rapidly. This growth substantially amplifies quadratic attention complexity and KV-cache overhead in the LLM, as demonstrated by LLaVA-NeXT [17], LLaVA-OneVision [18], and Qwen2-VL [19]. To enhance fine-grained perception without prohibitive token costs, MRA [20] adopts multi-resolution pathways to selectively attend to fine-grained tokens, Mini-Gemini [21] employs a dual visual encoder where low-resolution tokens query high-resolution patches via patch-level information mining, and PuMer [22] progressively reduces visual and textual tokens through text-informed pruning and modality-aware merging. While architectural and operator-level optimizations (*e.g.*, windowed attention [23], fused kernels [24, 25, 26]) improve overall throughput, the visual token count entering the LLM remains a dominant cost factor, motivating dedicated token reduction techniques. Recent advances in efficient visual representation learning, including occlusion-based contrastive learning [27, 28], self-adaptive token bases [29], and robust spatial-concept alignment [30], have shown that visual features can be substantially compressed without sacrificing discriminative power. These principles have also proven effective in domain-specific tasks such as medical image interpretation [31, 32, 33], pathology token compression [34, 35], multimodal medical foundation models [36, 37] and vision-centric long-context compression [38], further motivating our capacity-constrained formulation for token pruning.

2.2 Visual Token Reduction

Token reduction in transformer models is commonly achieved through token pruning or token merging, and has been widely studied in vision transformers to reduce computation while preserving performance [39, 40, 41]. In VLMs, the efficiency bottleneck often shifts to the LLM prefill stage, where long visual-token prefixes substantially increase self-attention cost and KV storage [42]. Therefore, reducing prefix visual tokens becomes a direct lever for lowering latency and memory. A representative line of work performs plug-and-play, training-free token pruning right after the vision encoder. PruMerge [43] and FasterVLM [44] use vision-side statistics such as [CLS]-to-patch attention to score token saliency. Other training-free approaches emphasize representational coverage: DivPrune [45], DART [46], and Feather [47] select tokens to maximize diversity or to minimize duplication among the retained set, which can be more robust than pure importance ranking at high pruning ratios.

Beyond one-shot pruning, FitPrune [48], VTW [49], and Balanced Token Pruning [50] introduce calibration-based or staged schedules to balance local feature preservation and downstream effects, typically using a small calibration set or lightweight statistics. In contrast to post-encoder pruning, FastV [4] and SparseVLM [51] prune inside the LLM stack to exploit deeper semantic mixing, trading earlier compute for potentially better task retention. Recent analyses by FasterVLM [44], DART [46], and [52] highlight that pruning signal and evaluation protocol are critical: cross-attention can be a noisy proxy for token importance, and naive baselines may be surprisingly competitive. From an engineering standpoint, strategies requiring dynamic token selection inside transformer blocks can complicate integration with optimized kernels like FlashAttention [24, 25, 26], whereas prefix-only pruning is often easier to deploy [46].

The pruning location also interacts with the accuracy–speed trade-off. Late pruning leverages higher-level semantics but reduces achievable end-to-end speedup, while early pruning maximizes savings but risks discarding fine-grained evidence needed for text-rich or localization-sensitive queries [4, 49, 53, 54]. Finally, [CLS]-based scoring methods such as PruMerge [43] and FasterVLM [44] implicitly assume the backbone provides such a token, which may not hold for modern architectures like Qwen2.5-VL [55], whose vision encoder lacks a [CLS] token.

Several recent methods learn token selection end-to-end rather than relying on fixed heuristics. GlimpsePrune [56] trains a visual importance predictor before answer generation; however, its optimization relies heavily on bounding box annotations, tying pruning to a localization surrogate and potentially limiting generalization to open-vocabulary tasks. ATP-LLaVA [10] incorporates adaptive modules between LLM layers to predict instance-wise retention ratios. Although it uses differentiable approximations to bypass hard selection, it still requires complex auxiliary losses to enforce pruning budgets. Taking a different direction, p-MoD [57] applies Mixture-of-Depths routing to vision tokens. Ensuring convergence requires joint fine-tuning of the entire LLM backbone, an intrusive process risking disruption of pre-trained language priors. Together with the heuristic limitations discussed above, these observations motivate a pruning formulation that is data-driven yet non-intrusive to the base model.

3 Methodology

3.1 Overview of the Framework

Given an input image \mathbf{I} , a frozen vision encoder \mathcal{E}_v produces N visual token embeddings $\mathbf{X}^v = \mathcal{E}_v(\mathbf{I}) \in \mathbb{R}^{N \times d_v}$, transformed by a projector $\mathbf{P}_{v \rightarrow \ell}$ and concatenated with text embeddings $\mathcal{E}_t(\mathbf{T})$ before being fed to the frozen LLM

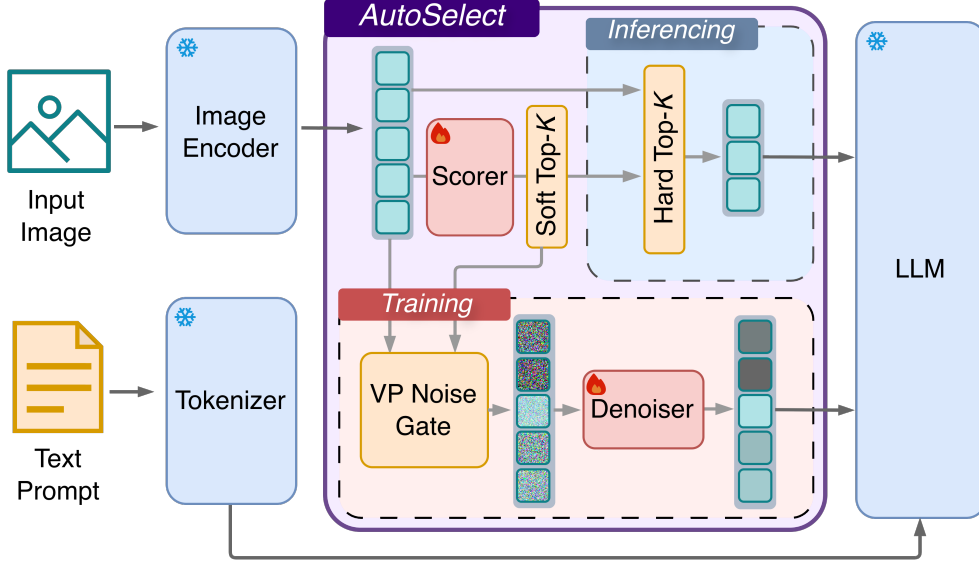


Figure 2: **Overview of the AutoSelect framework.** Visual tokens from the frozen Image Encoder pass through a learnable Scorer that assigns per-token importance scores. These scores are polarized by the differentiable *Soft Top-K* operator under a fixed bandwidth budget K . *During training* (lower path), a VP Noise Gate injects variance-preserving noise into each token in inverse proportion to its score; the Denoiser then maps the perturbed sequence back toward the LLM’s expected input space. *At inference* (upper path), the Denoiser and noise injection are discarded: Hard Top- K retains the K highest-scoring tokens with their original position indices. All base VLM parameters, including the Image Encoder, modality projector, and LLM, remain frozen.

\mathcal{L} . Since the vision encoder accounts for less than 5% of total inference cost while the LLM dominates, we place our pruning module after the encoder and before the projector to maximize computational savings.

As illustrated in Figure 2, our framework introduces two lightweight modules, a **Scorer** $\mathcal{S}(\cdot)$ and a **Denoiser** $\mathcal{D}(\cdot)$, which are jointly trained and placed between the encoder and the projector, while all original VLM parameters remain frozen. The entire framework is optimized end-to-end using the standard language modeling objective, without requiring auxiliary losses or hand-crafted features.

Training phase. The Scorer assigns per-token importance scores that are polarized by a differentiable *Soft Top-K* operator under a fixed bandwidth K . Rather than removing tokens, we inject variance-preserving (VP) noise with magnitude inversely proportional to each token’s polarized score, keeping the sequence length at N . The perturbed sequence is processed by the Denoiser and forwarded through the frozen projector and LLM. Only the Scorer parameters θ and Denoiser parameters ϕ are optimized via the negative log-likelihood (NLL) loss for next-token prediction:

$$\min_{\theta, \phi} \mathcal{J}_{\text{NLL}} \left(\mathcal{L} \left([\mathcal{D}_{\phi}(\tilde{\mathbf{X}}^v) \mathbf{P}_{v \rightarrow \ell}; \mathcal{E}_t(\mathbf{T})] \right), \{y_t^*\} \right), \quad (1)$$

where $\tilde{\mathbf{X}}^v$ denotes the noise-gated visual sequence (Equation (5)) and $\{y_t^*\}$ the ground-truth targets.

Inference phase. At inference time, the Denoiser and noise injection are removed entirely. The Scorer produces importance scores, and a standard hard top- K operation selects the K highest-scoring tokens:

$$\hat{\mathbf{X}}^v = \text{Top-K}(\mathbf{X}^v, \mathcal{S}(\mathbf{X}^v), K) \in \mathbb{R}^{K \times d_v}, \quad (2)$$

where the selected tokens retain their original position indices rather than being re-indexed sequentially. This design ensures that the rotary position embeddings (RoPE) within the LLM correctly encode each retained token’s spatial location in the image grid. Because the Scorer operates only on visual features, it is text-agnostic: importance scores do not depend on the language prompt and can be reused across dialogue turns without re-evaluation.

3.2 Learnable Token Scorer with Soft Top- K Selection

The Scorer $\mathcal{S}(\cdot)$ comprises L Transformer encoder blocks followed by a linear projection that maps each of the N visual tokens to a scalar importance score:

$$\mathbf{s} = \mathcal{S}(\mathbf{X}^v) \in \mathbb{R}^N. \quad (3)$$

A standard hard top- K is piecewise constant and produces zero gradients almost everywhere, preventing effective Scorer training. We therefore employ the differentiable Soft Top- K operator Φ_K [58]. Raw scores are first z-score normalized for numerical stability, then mapped through Φ_K :

$$\boldsymbol{\alpha} = \Phi_K(\hat{\mathbf{s}} / \tau) \in [0, 1]^N, \quad \text{with} \quad \sum_{i=1}^N \alpha_i \approx K, \quad (4)$$

where $\hat{\mathbf{s}}$ denotes the normalized scores and $\tau > 0$ is a temperature parameter. Conceptually, Φ_K is closer to softmax than to hard top- K : both are smooth, temperature-scaled maps from \mathbb{R}^N to $[0, 1]^N$. The distinction is in the normalizing constraint—softmax imposes $\sum_i \alpha_i = 1$, whereas Φ_K fixes $\sum_i \alpha_i = K$, turning the operator into a budget-constrained soft assignment. A data-dependent threshold further separates Φ_K from softmax: scores are driven toward 0 or 1, so the output is bimodal rather than spread across all tokens. Because the budget is fixed, the Scorer learns *which* tokens to retain, not *how many*. We anneal τ from τ_{start} to τ_{end} on a cosine schedule; at large τ the scores are diffuse, and as $\tau \rightarrow 0$ they collapse to the binary mask used at inference.

3.3 Capacity-Constrained Gating via Noise Injection

Given the polarized importance scores $\boldsymbol{\alpha}$ from the Soft Top- K operator, we now describe how they are used to modulate the information content of each token during training. A naïve approach would be to directly remove low-scoring tokens; however, this would reduce the sequence length and introduce a non-differentiable discontinuity that disrupts gradient flow. Instead, we keep all N tokens but impose token-wise capacity constraints through noise injection: the effective information that each token can transmit to the downstream LLM is reduced in proportion to its importance score.

Concretely, we adopt a variance-preserving (VP) noise injection scheme. For the i -th visual token $\mathbf{x}_i^v \in \mathbb{R}^{d_v}$, the gated representation is computed as:

$$\tilde{\mathbf{x}}_i = \sqrt{\alpha_i} \mathbf{x}_i^v + \sqrt{1 - \alpha_i} \boldsymbol{\epsilon}_i, \quad \boldsymbol{\epsilon}_i \sim \mathcal{N}(\mathbf{0}, \mathbf{I}), \quad (5)$$

where $\alpha_i \in [0, 1]$ is the polarized score from Equation (4) and $\mathbf{I} \in \mathbb{R}^{d_v \times d_v}$ is the identity matrix. This formulation admits a direct information-theoretic interpretation. When $\alpha_i \rightarrow 1$ (high importance), the noise component vanishes and the original token is preserved; when $\alpha_i \rightarrow 0$ (low importance), the signal is replaced by isotropic Gaussian noise. Intermediate values interpolate between these extremes, providing a differentiable proxy for discrete token removal.

Because the vision encoder output passes through layer normalization, the coefficients $\sqrt{\alpha_i}$ and $\sqrt{1 - \alpha_i}$ ensure $\text{Var}(\tilde{\mathbf{x}}_i) \approx \text{Var}(\mathbf{x}_i^v)$, keeping the feature scale stable and preventing distribution shifts for the frozen LLM. The Scorer therefore determines the noise level of each token, and thus its effective capacity, according to its estimated importance. We empirically verify that VP noise gating approximates the information restriction of hard Top- K pruning; quantitative and qualitative comparisons are shown in Figure 5 (Section 4.6).

3.4 Lightweight Denoiser with Diagonal Attention

Although the VP formulation preserves marginal variance, it shifts token distributions in feature space, particularly for low-importance tokens approaching isotropic Gaussian noise. To map the perturbed sequence back toward the input distribution expected by the LLM, we introduce a lightweight Denoiser $\mathcal{D}(\cdot)$ consisting of a single Transformer encoder block.

If standard global self-attention were used, high-importance tokens could leak information to low-importance ones, undermining the capacity constraints imposed by noise injection. We therefore adopt diagonal attention: an identity attention mask restricts each token to attend only to itself, so the self-attention layer degenerates into a per-token nonlinear transformation through the value projection and feed-forward network independently. This prevents cross-token information leakage while enabling a learned per-token mapping from the noise-perturbed space to the LLM-compatible manifold. The Denoiser is used only during training; at inference no noise is injected and only the top- K tokens are retained, so the Denoiser adds zero overhead.

4 Experiments

4.1 Experimental Setup

The Scorer and Denoiser are jointly trained on ImageNet-1K [59] captioning data from ImageNet-1K-VL-Enriched [60], adding $\sim 84\text{M}$ trainable parameters while all base VLM weights remain frozen. We evaluate on three architectures: LLaVA-v1.5-7B [3], LLaVA-NeXT-7B [61], and Qwen2.5-VL-7B [55]. Full training hyperparameters and implementation details are provided in the supplementary material.

Benchmarks. We evaluate on ten standard VLM benchmarks: GQA [62], MMBench [63], MMBench-CN [63], MME [64], POPE [65], ScienceQA-IMG [66], VQAv2 [67], TextVQA [68], SEED-Bench [69], and VizWiz [70]. This set follows the evaluation protocol used by DivPrune [45], SparseVLM [51], and HoloV [71], allowing direct comparison; detailed benchmark descriptions are provided in the supplementary material. In all tables, the ‘‘Avg.’’ column reports *average performance retention*: for each benchmark, we compute the ratio of the pruned model’s score to the unpruned upper bound, then average these ratios.

Baselines. We organize baselines by where pruning occurs, as this directly governs the accuracy–efficiency trade-off. 1) **Pre-LLM pruning** (same location as AutoSelect): tokens are selected or merged before the LLM, so every LLM layer processes only K visual tokens. Methods: ToMe [39], HiRED [72], DivPrune [45], VisionZip [5], HoloV [71], and PRUNESID [73]. 2) **In-LLM pruning**: tokens are pruned inside the LLM (typically at layer 2–4); the first few LLM layers still see all N tokens, which retains more information at the cost of less end-to-end speedup. Methods: FastV [4], SparseVLM [51], DART [46], and PDrop [74]. We report the pruning location alongside accuracy in every table so that readers can account for this structural difference when comparing results (*cf.* Section 4.4).

4.2 Main Benchmark Results Across Models

Results on LLaVA-1.5-7B. To ensure a direct comparison with prior literature, we establish LLaVA-1.5-7B as our primary testbed. In this architecture, the vision encoder processes input images at 336×336 resolution, yielding a sequence of 576 visual tokens. Table 1 presents the comparison on LLaVA-1.5-7B across ten benchmarks. We group methods by pruning location (Pre-LLM vs. In-LLM) to facilitate fair interpretation. We evaluate three compression regimes, retaining 192, 128, and 64 tokens, corresponding to progressively more aggressive reductions from the original 576 tokens. When retaining 192 tokens, our method achieves performance on par with the strongest baselines and is slightly below PRUNESID [73] in average accuracy. However, this gap should be interpreted together with the efficiency analysis in Section 4.4. PRUNESID [73] incurs substantially higher overhead in determining which tokens to preserve, which offsets its small performance advantage. As the token budget decreases, the advantage of AutoSelect becomes more evident. At 128 tokens, AutoSelect surpasses all baselines in average retention. Under extreme compression at 64 tokens, AutoSelect reaches 96.5% average retention, exceeding PRUNESID [73] by 1.4%. This suggests that the capacity-constrained formulation is particularly effective at identifying informative token subsets when the budget is limited.

Results on LLaVA-NEXT-7B. To evaluate scalability under higher visual loads, we extend our analysis to LLaVA-NEXT-7B, which raises the input resolution to 672×672 and produces 2,880 visual tokens—a $5 \times$ increase over LLaVA-1.5. This longer sequence amplifies the LLM prefill bottleneck, making effective token reduction both more critical and more challenging. We retain only 320 tokens (88.9% reduction). As shown in Table 2, AutoSelect achieves 96.1% average performance retention, outperforming the strongest baseline (HoloV, 95.7%) by 0.4%, confirming that our capacity-constrained scoring mechanism generalizes well to substantially larger token pools without degradation.

Results on Qwen2.5-VL-7B. We further evaluate on Qwen2.5-VL-7B [55], which differs from LLaVA in vision encoder, projector, and LLM backbone. Qwen2.5-VL processes images at native resolution, so the visual token count varies per image; we therefore report results by pruning rate rather than a fixed token budget. As shown in Table 3, AutoSelect outperforms all baselines across all three pruning rates. Because the Scorer operates on per-token features without assumptions about grid layout or fixed sequence length, the same architecture and training recipe apply directly to Qwen’s variable-length setting. This indicates that the method generalizes beyond the LLaVA family.

4.3 LLM-Free Evaluation of Pruning Quality

Because the Scorer operates entirely on visual features, its selection quality can be measured without the LLM. Each method first scores all $N=576$ tokens on the 24×24 grid produced by CLIP ViT-L/14 and generates a binary selection mask for budget K . This mask is then resized from 24×24 to 14×14 to match the patch grid of a separately trained

Table 1: **Results on LLaVA-1.5-7B under different token budgets.** “Loc.” denotes pruning location (Pre = before LLM; L_a-L_b = from LLM layer a to b). Upper bound uses all 576 visual tokens; remaining blocks report 192/128/64 retained tokens (66.7%/77.8%/88.9% pruning). “Avg.” is the mean ratio of each benchmark score to its upper bound. **Formatting:** within each Retain- K block, the best Avg. is colored **red** and the second best is colored **blue**; our method is highlighted in **blue**.

Method	Loc.	GQA	MMB	MMB _{CN}	MME	POPE	SQA	VQA ^{v2}	VQA ^{Text}	SEED	VizWiz	Avg.
<i>Upper Bound, 576 Tokens (100%)</i>												
Vanilla	-	61.9	64.7	58.1	1862	85.9	69.5	78.5	58.2	60.5	54.3	100%
<i>Retain 192 Tokens (66.7% pruning)</i>												
ToMe (ICLR’23)	Pre	54.3	60.5	-	1563	72.4	65.2	68.0	52.1	-	-	88.5%
FastV (ECCV’24)	L2-L32	52.7	61.2	53.5	1612	64.8	67.3	67.1	52.5	57.1	50.8	89.4%
SparseVLM (ICML’25)	L1-L32	57.6	62.5	58.6	1721	83.6	69.1	75.6	56.1	55.8	50.5	95.8%
DART (EMNLP’25)	L2	60.0	63.6	57.1	1856	82.8	69.8	76.7	57.4	51.5	54.9	97.3%
HiRED (AAAI’25)	Pre	58.7	62.8	54.7	1737	82.8	68.4	74.9	47.4	-	50.1	93.7%
PDrop (CVPR’25)	L8-L24	57.3	63.6	56.8	1797	82.3	69.2	75.1	56.5	54.7	-	96.0%
DivPrune (CVPR’25)	Pre	60.0	62.3	-	1752	87.0	68.7	75.5	56.4	58.6	55.6	97.8%
VisionZip (CVPR’25)	Pre	59.3	63.0	57.3	1783	85.3	68.9	76.8	57.3	58.5	54.1	97.9%
HoloV (NeurIPS’25)	Pre	59.0	65.4	58.0	1820	85.6	69.8	76.7	57.4	-	50.9	98.2%
PRUNESID (ICLR’26)	Pre	60.1	63.7	-	1791	86.9	68.5	76.8	56.7	59.0	55.4	98.5%
AutoSelect (Ours)	Pre	57.8	63.4	57.5	1791	86.5	70.2	76.6	55.3	59.2	55.9	98.2%
<i>Retain 128 Tokens (77.8% pruning)</i>												
ToMe (ICLR’23)	Pre	52.4	53.3	-	1343	62.8	59.6	63.0	49.1	-	-	80.4%
FastV (ECCV’24)	L2-L32	49.6	56.1	55.9	1490	59.6	60.2	61.8	50.6	55.9	51.3	85.2%
SparseVLM (ICML’25)	L1-L32	56.0	60.0	51.1	1696	80.5	67.1	73.8	54.9	53.4	51.4	92.4%
DART (EMNLP’25)	L2	58.7	63.2	57.3	1840	80.1	69.1	75.9	56.4	50.5	55.3	96.2%
HiRED (AAAI’25)	Pre	57.2	61.5	53.6	1710	79.8	68.1	73.4	46.1	-	51.3	92.2%
PDrop (CVPR’25)	L8-L24	57.1	61.6	56.6	1761	82.3	68.4	72.9	56.6	53.3	-	94.7%
DivPrune (CVPR’25)	Pre	59.2	62.3	54.8	1752	86.9	69.0	74.7	56.0	57.1	55.6	96.9%
VisionZip (CVPR’25)	Pre	57.6	62.0	56.7	1762	83.2	68.9	75.6	56.8	57.1	54.5	96.6%
HoloV (NeurIPS’25)	Pre	57.7	63.9	56.5	1802	82.8	69.8	75.5	56.8	-	51.5	96.8%
PRUNESID (ICLR’26)	Pre	58.8	62.1	-	1749	86.5	68.3	75.3	54.7	57.8	55.8	96.9%
AutoSelect (Ours)	Pre	57.5	62.9	57.4	1765	85.7	70.2	76.1	54.9	58.4	56.1	97.6%
<i>Retain 64 Tokens (88.9% pruning)</i>												
ToMe (ICLR’23)	Pre	48.6	43.7	-	1138	52.5	50.0	57.1	45.3	-	-	70.1%
FastV (ECCV’24)	L2-L32	46.1	48.0	52.7	1256	48.0	51.1	55.0	47.8	51.9	50.8	76.8%
SparseVLM (ICML’25)	L1-L32	52.7	56.2	46.1	1505	75.1	62.2	68.2	51.8	51.1	53.1	86.7%
DART (EMNLP’25)	L2	55.9	60.6	53.6	1765	73.9	69.8	72.4	54.4	47.2	55.3	92.3%
HiRED (AAAI’25)	Pre	54.6	60.2	53.0	1599	73.6	68.2	68.7	44.2	-	50.2	88.7%
PDrop (CVPR’25)	L8-L24	47.5	58.8	50.5	1561	55.9	69.0	69.2	50.6	40.0	-	82.7%
DivPrune (CVPR’25)	Pre	57.6	59.3	53.7	1638	85.6	68.3	72.9	55.5	55.4	57.5	94.9%
VisionZip (CVPR’25)	Pre	55.1	60.1	50.4	1690	77.0	69.0	72.4	55.5	54.5	54.8	92.7%
HoloV (NeurIPS’25)	Pre	55.3	63.3	55.1	1715	80.3	69.5	72.8	55.4	-	52.8	94.8%
PRUNESID (ICLR’26)	Pre	57.1	58.8	-	1733	83.8	67.8	73.7	54.2	56.1	56.9	95.1%
AutoSelect (Ours)	Pre	56.8	62.6	56.6	1723	83.4	70.1	73.9	54.3	57.6	57.2	96.5%

ViT-B/16, and unselected patches are discarded *before* patch embedding, so the classifier sees only the chosen subset. The ViT-B/16 is a MAE-pretrained model fine-tuned on ImageNet-1K. Top-1 and Top-5 accuracy are reported for K from 6 to 64. We compare against FastV [4] and HoloV [71], representing in-LLM and pre-LLM pruning baselines respectively.

Figure 3 shows that AutoSelect surpasses both FastV and HoloV at every budget in both Top-1 and Top-5 accuracy. The margin is widest under heavy pruning: at $K=6$ (3% of tokens) AutoSelect leads HoloV by roughly 10 percentage points in Top-1, while FastV trails further behind. As the budget grows the three methods gradually converge, yet AutoSelect maintains a consistent advantage at $K=64$. This is expected: when only a handful of tokens survive, attention-based heuristics (FastV) and handcrafted scoring (HoloV) struggle to cover enough semantic content, whereas the learned Scorer can still place its budget on the most informative patches. Because the experiment bypasses the LLM entirely, it confirms that the accuracy gains in Section 4.2 originate from better token selection rather than from LLM adaptation.

Table 2: **Results on LLaVA-NEXT-7B.** “Loc.” denotes pruning location (Pre = before LLM; L_a – L_b = from LLM layer a to b). “Avg.” is the mean ratio of each benchmark score to its upper bound. **Formatting:** the best Avg. is colored red and the second best is colored blue; our method is highlighted in blue.

Method	Loc.	GQA	MMB	MMB _{CN}	MME	POPE	SQA	VQA ^{v2}	VQA ^{Text}	Avg.
<i>Upper Bound, 2880 Tokens (100%)</i>										
Vanilla	-	64.2	67.4	60.6	1851	86.5	70.1	80.8	64.9	100%
<i>Retain 320 Tokens (88.9% pruning)</i>										
FastV (ECCV’24)	L2–L32	55.9	61.6	51.9	1661	71.7	62.8	71.9	55.7	87.6%
PDrop (CVPR’25)	L8–L24	56.4	63.4	56.2	1663	77.6	67.5	73.5	54.4	90.7%
DART (EMNLP’25)	L2	61.7	65.3	58.2	1710	84.1	68.4	79.1	58.7	95.6%
HiRED (AAAI’25)	Pre	59.3	64.2	55.9	1690	83.3	66.7	75.7	58.8	93.4%
HoloV (NeurIPS’25)	Pre	61.7	65.3	57.5	1738	83.9	68.9	79.5	58.7	95.7%
AutoSelect (Ours)	Pre	62.3	64.7	57.4	1723	85.9	72.7	78.6	56.7	96.1%

Table 3: **Results on Qwen2.5-VL-7B.** “Avg.” is the mean ratio of each benchmark score to its upper bound. **Formatting:** the best Avg. is colored red and the second best is colored blue; our method is highlighted in blue.

Method	MMB	MME	POPE	SQA	VQA ^{Text}	Avg.
<i>Upper Bound (100%)</i>						
Vanilla	82.8	2304	86.1	84.7	84.8	100%
<i>Token Pruning Rate = 66.7%</i>						
FastV (ECCV’24)	75.7	2072	82.2	78.5	77.9	92.3%
HoloV (NeurIPS’25)	78.3	2093	85.0	79.8	78.9	94.3%
AutoSelect (Ours)	81.7	2279	84.9	86.4	79.0	98.3%
<i>Token Pruning Rate = 77.8%</i>						
FastV (ECCV’24)	74.9	2036	80.7	78.0	69.0	89.2%
HoloV (NeurIPS’25)	76.5	2043	82.3	79.8	70.3	90.8%
AutoSelect (Ours)	81.0	2218	82.8	83.7	76.7	95.9%
<i>Token Pruning Rate = 88.9%</i>						
FastV (ECCV’24)	69.2	1940	78.6	77.4	60.3	84.3%
HoloV (NeurIPS’25)	72.4	2006	80.7	79.5	61.8	87.0%
AutoSelect (Ours)	76.7	2113	79.8	82.9	76.7	93.1%

4.4 Efficiency Analysis

We profile all methods on LLaVA-1.5-7B with 336×336 inputs and $N=576$ visual tokens on a single NVIDIA A6000 GPU under batch size 1 with FP16 precision. FLOPs are measured via PyTorch Profiler, and latencies are averaged over 30 forward passes after warmup. To pinpoint savings, we decompose time-to-first-token (TTFT) into three stages: *Vision Encoding*, covering the vision-tower forward pass; *Pruning Module*, capturing token selection overhead; and *LLM Prefill*, measuring the language-model forward pass over retained tokens.

As shown in Table 4, vision encoding cost is nearly identical at approximately 30 ms, since none prune tokens inside the encoder. Key differences emerge subsequently. PyramidDrop drops tokens at layers 8, 16, and 24; earlier layers attend over the full visual prefix, resulting in LLM prefill of 70.08 ms and 4.89 T FLOPs. The three Pre-LLM methods, PruneSID, HoloV, and AutoSelect, reduce tokens before the LLM and share similar prefill costs of approximately 40 ms and 2.1 T FLOPs. Among them, pruning overhead becomes decisive. PruneSID’s module requires 43.39 ms, over $60 \times$ slower than AutoSelect, pushing its prefill total to 115.84 ms, barely faster than using all tokens. HoloV’s module costs

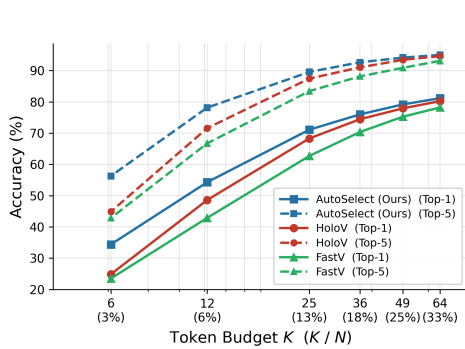


Figure 3: **LLM-free classification on ImageNet-1K.** Each method generates a selection mask on 24×24 token grid, which is resized to 14×14 and applied to a ViT-B/16 by removing unselected patches before embedding.

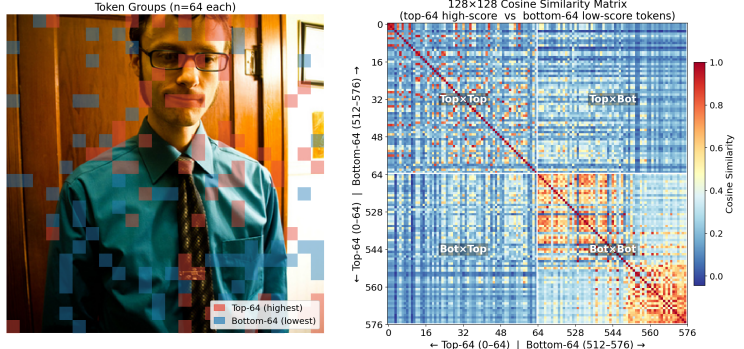


Figure 4: **Token selection and pairwise similarity ($K=64$).** Red/blue patches denote the 64 highest-/lowest-scored tokens. The 128×128 cosine-similarity matrix is arranged as [top-64 | bottom-64]. Retained tokens (upper-left block) are dissimilar; pruned tokens (lower-right block) are highly similar.

Table 4: **Efficiency and prefill-stage breakdown on LLaVA-1.5-7B ($K=64$).** “Loc.” denotes pruning location, consistent with previous tables. Prefill Total is time-to-first-token (TTFT). All latencies are in milliseconds, averaged over 30 forward passes.

Method	Loc.	K	FLOPs (T)	Vision Enc. (ms)	Pruning Module (ms)	LLM Prefill (ms)	Prefill Total (ms)
Full (LLaVA)	—	576	8.89	29.71	0.00	118.66	149.51
PruneSID	Pre	64	2.13	31.80	43.39	39.74	115.84
PyramidDrop	L8–L24	64	4.89	29.54	5.02	70.08	105.90
HoloV	Pre	64	2.15	31.96	2.77	41.48	77.39
AutoSelect (Ours)	Pre	64	2.13	29.41	0.69	41.61	72.73

2.77 ms, roughly $4 \times$ that of AutoSelect. By contrast, AutoSelect completes token selection in 0.69 ms and achieves the lowest TTFT of 72.73 ms.

4.5 Visualization

Figure 4 visualizes the Scorer’s decisions on a sample image. In the left panel, high-score tokens (red) cover the subject’s face, hands, and clothing texture, while low-score tokens (blue) land on the wooden background and plain shirt regions where neighbouring patches look alike. The right panel makes this difference quantitative. We compute cosine similarity between the 64 highest- and 64 lowest-scored tokens and arrange the resulting 128×128 matrix in block form. The Top \times Top block (upper left) is predominantly blue: retained tokens are far apart in feature space, meaning each one carries distinct information. The Bot \times Bot block (lower right) is red: pruned tokens cluster tightly, so removing them costs little unique information. The capacity-constrained training thus pushes the Scorer to spread its budget across tokens that are far apart in feature space, rather than wasting it on near-duplicates.

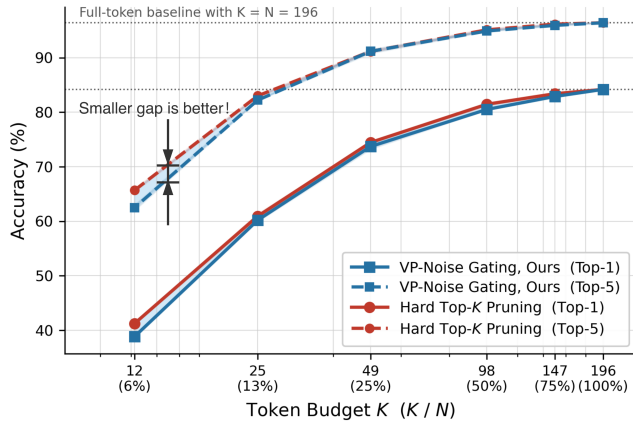
4.6 Ablation Studies

We ablate the two core design choices of our training framework, namely VP noise gating and diagonal attention in the Denoiser, on LLaVA-1.5-7B across three token budgets ($K=64, 128, 192$). For each configuration, we report the average performance retention over four benchmarks (GQA, MMB, POPE, MME) as summarized in Table 5. The base configuration (VP noise gating + diagonal attention) serves as our default; each variant modifies exactly one design choice.

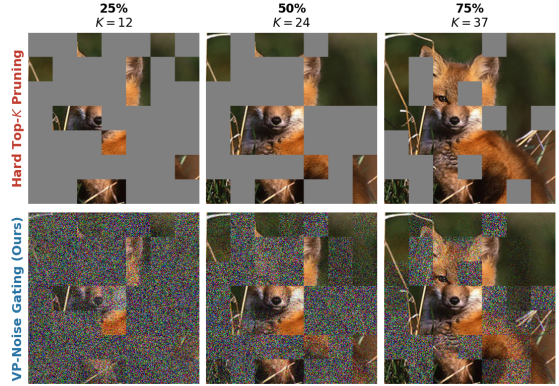
VP noise gating vs. scale gating. The central mechanism of our training framework is variance-preserving noise injection, which modulates each token’s information throughput via $\mathbf{x}' = \sqrt{\alpha} \mathbf{x} + \sqrt{1 - \alpha} \epsilon$. A natural alternative is direct scale gating, $\mathbf{x}' = \alpha \cdot \mathbf{x}$, which simply attenuates low-score tokens toward zero. Table 5 shows that replacing VP noise with scale gating degrades performance across all token budgets, with the gap widening under aggressive

Table 5: **Ablation studies** on LLaVA-1.5-7B. Each row reports the average performance retention (%) over GQA, MMB, POPE, and MME across three token budgets. “Base” denotes the full AutoSelect configuration (VP noise + diagonal attention).

Configuration	Modification	$K=64$	$K=128$	$K=192$
Base (VP noise + diagonal) [†]	–	95.5%	97.3%	98.3%
Global attention	diagonal → global	92.7% (-2.8)	95.0% (-2.3)	95.9% (-2.4)
Scale gating	VP noise → scale	93.2% (-2.3)	94.8% (-2.5)	96.5% (-1.8)



(a) Top-1 (solid) and Top-5 (dashed) accuracy on ImageNet-1K validation as a function of token budget K . Shaded regions indicate the gap between the two strategies. Dotted lines mark the full-token baseline ($K=N$).



(b) Visualization under three retention levels with $N=49$ tokens ($K \in \{12, 24, 37\}$, corresponding to $\sim 25\%$, 50% , and 75% retention). *Top*: hard Top- K masking keeps the K selected patches while graying out the rest. *Bottom*: VP-noise gating retains all positions but injects score-proportional noise, producing a soft selection effect.

Figure 5: **Validation of VP-noise gating as a differentiable proxy for hard Top- K pruning.** Both strategies are applied after patch embedding and before the vision encoder, matching the insertion point used by AutoSelect. Both use identical random score maps to control for scoring quality. Quantitatively (a) and qualitatively (b), the two mechanisms produce equivalent information restriction across all budget levels, justifying VP-noise gating as a continuous, gradient-friendly training surrogate.

pruning ($K=64$: 95.5% vs. 93.2%). Scale gating reduces the magnitude of low-importance tokens but preserves their directional information intact, allowing the downstream LLM to partially recover the attenuated content through its layernorm and attention mechanisms. VP noise gating, by contrast, actively corrupts the representational content of low-score tokens with isotropic noise, creating a hard capacity constraint during training: the only way for the system to preserve task-relevant information is to assign high importance scores to the corresponding tokens. This creates a stronger learning signal for the Scorer, resulting in more discriminative importance allocation.

Diagonal vs. global attention in the Denoiser. Replacing diagonal attention with global self-attention causes the largest degradation across all budgets (Table 5), confirming the information-leakage hypothesis. With global attention, heavily noised tokens can attend to high-score tokens and recover information that should have been suppressed, effectively circumventing the capacity constraint imposed by the noise gating stage. Diagonal attention enforces strict per-token independence, ensuring that each token’s information throughput is determined solely by its importance score. This design is essential for maintaining the integrity of the capacity-constrained formulation during training.

VP noise gating vs. hard Top- K pruning. We empirically verify that VP noise gating imposes information constraints similar to discrete removal. Using a random scorer to isolate the gating mechanism, Figure 5a shows that both strategies produce nearly identical accuracy degradation on ImageNet-1K across token budgets. The narrow shaded gap in Figure 5a confirms that VP noise gating closely matches the information restriction imposed by hard Top- K , and Figure 5b provides a visual comparison at matched retention levels.

5 Conclusion

We presented AutoSelect, a framework that recasts visual token pruning as capacity-constrained representation learning. By modulating per-token information throughput via variance-preserving noise rather than discarding tokens outright, the framework turns discrete pruning into a continuous optimization problem trained end-to-end with the standard next-token prediction loss as the sole objective, requiring no auxiliary losses. A diagonal-attention Denoiser prevents information leakage across tokens during training and is removed at inference, adding zero overhead. On LLaVA-1.5-7B, AutoSelect retains 96.5% of full-model accuracy at 88.9% token pruning with only 0.69 ms selection overhead, and generalizes without architecture-specific modification to LLaVA-NEXT and Qwen2.5-VL, consistently outperforming existing methods across all evaluated settings. These results indicate that learned capacity allocation can replace heuristic pruning criteria: given a fixed bandwidth budget and a differentiable relaxation, the model discovers which visual tokens carry task-relevant information.

References

- [1] Junnan Li, Dongxu Li, Silvio Savarese, and Steven Hoi. Blip-2: Bootstrapping language-image pre-training with frozen image encoders and large language models. In *Proceedings of the 40th International Conference on Machine Learning (ICML)*, pages 19730–19742. PMLR, 2023.
- [2] Wenliang Dai, Junnan Li, Dongxu Li, Anthony Meng Huat Tiong, Junqi Zhao, Weisheng Wang, Boyang Li, Pascale Fung, and Steven Hoi. Instructblip: Towards general-purpose vision-language models with instruction tuning. In *Advances in Neural Information Processing Systems (NeurIPS) 36*, 2023.
- [3] Haotian Liu et al. LLaVA: Large language and vision assistant for visual instruction tuning. In *Advances in Neural Information Processing Systems (NeurIPS) 36*, 2023.
- [4] Liang Chen, Haozhe Zhao, Tianyu Liu, Shuang Bai, Junyang Lin, Chang Zhou, and Baobao Chang. An image is worth 1/2 tokens after layer 2: Plug-and-play inference acceleration for large vision-language models. In *Proceedings of the European Conference on Computer Vision (ECCV)*, 2024.
- [5] Senqiao Yang, Yukang Chen, Zhuotao Tian, Chengyao Wang, Jingyao Li, Bei Yu, and Jiaya Jia. Visionzip: Longer is better but not necessary in vision language models. In *Proceedings of the IEEE/CVF Conference on Computer Vision and Pattern Recognition (CVPR)*, pages 19792–19802, 2025.
- [6] Cheng Yang, Yang Sui, Jinqi Xiao, Lingyi Huang, Yu Gong, Chendi Li, Jinghua Yan, Yu Bai, Ponnuswamy Sadayappan, Xia Hu, and Bo Yuan. Topv: Compatible token pruning with inference time optimization for fast and low-memory multimodal vision language model. In *Proceedings of the IEEE/CVF Conference on Computer Vision and Pattern Recognition (CVPR)*, pages 19803–19813, 2025.
- [7] Shiyu Zhao, Zhenting Wang, Felix Juefei-Xu, Xide Xia, Miao Liu, Xiaofang Wang, Mingfu Liang, Ning Zhang, Dimitris N. Metaxas, and Licheng Yu. Accelerating multimodal large language models by searching optimal vision token reduction. In *Proceedings of the IEEE/CVF Conference on Computer Vision and Pattern Recognition (CVPR)*, pages 29869–29879, 2025.
- [8] Kai Huang, Hao Zou, Ye Xi, BoChen Wang, Zhen Xie, and Liang Yu. Ivtp: Instruction-guided visual token pruning for large vision-language models. In *Proceedings of the European Conference on Computer Vision (ECCV)*, pages 214–230, 2024.
- [9] Jianjian Cao, Peng Ye, Shengze Li, Chong Yu, Yansong Tang, Jiwen Lu, and Tao Chen. Madtp: Multimodal alignment-guided dynamic token pruning for accelerating vision-language transformer. In *Proceedings of the IEEE/CVF Conference on Computer Vision and Pattern Recognition (CVPR)*, pages 15710–15719, 2024.
- [10] Xubing Ye, Yukang Gan, Yixiao Ge, Xiao-Ping Zhang, and Yansong Tang. Atp-llava: Adaptive token pruning for large vision language models. In *Proceedings of the IEEE/CVF Conference on Computer Vision and Pattern Recognition (CVPR)*, pages 24972–24982, 2025.
- [11] Haozhan Shen, Peng Liu, Jingcheng Li, Chunxin Fang, Yibo Ma, Jiajia Liao, Qiaoli Shen, Zilun Zhang, Kangjia Zhao, Qianqian Zhang, et al. Vlm-r1: A stable and generalizable r1-style large vision-language model. *arXiv preprint arXiv:2504.07615*, 2025.
- [12] Wonkyun Kim, Changin Choi, Wonseok Lee, and Wonjong Rhee. An image grid can be worth a video: Zero-shot video question answering using a vlm. *IEEE Access*, 12:193057–193075, 2024.
- [13] Hu Xu, Gargi Ghosh, Po-Yao Huang, Prahal Arora, Masoumeh Aminzadeh, Christoph Feichtenhofer, Florian Metze, and Luke Zettlemoyer. Vlm: Task-agnostic video-language model pre-training for video understanding. In *Findings of the Association for Computational Linguistics: ACL-IJCNLP 2021*, pages 4227–4239, 2021.

- [14] Yan Zeng, Xinsong Zhang, Hang Li, Jiawei Wang, Jipeng Zhang, and Wangchunshu Zhou. X²-vlm: All-in-one pre-trained model for vision-language tasks. *IEEE transactions on pattern analysis and machine intelligence*, 46(5):3156–3168, 2023.
- [15] Jean-Baptiste Alayrac et al. Flamingo: a visual language model for few-shot learning, 2022.
- [16] Zhiyuan Zhang et al. Unveiling encoder-free vision-language models. In *NeurIPS*, 2024.
- [17] Xin Li et al. LLaVA-next-interleave: Tackling multi-image, video, and 3d in large multimodal models, 2025. ICLR.
- [18] Xin Li et al. LLaVA-onevision: Easy visual task transfer, 2024. arXiv preprint.
- [19] Qwen Team. Qwen2-VL: Enhancing vision-language model’s perception of the world at any resolution, 2024. arXiv preprint.
- [20] Jiahui Yu et al. Feast your eyes: Mixture-of-resolution adaptation for multimodal large language models, 2026. ICLR.
- [21] Yanwei Li, Yuechen Zhang, Chengyao Wang, Zhisheng Zhong, Yixin Chen, Ruihang Chu, Shaoteng Liu, and Jiaya Jia. Mini-gemini: Mining the potential of multi-modality vision language models. *IEEE Transactions on Pattern Analysis and Machine Intelligence*, 2025.
- [22] Qingqing Cao, Bhargavi Paranjape, and Hannaneh Hajishirzi. Pumer: Pruning and merging tokens for efficient vision language models. In *Proceedings of the 61st Annual Meeting of the Association for Computational Linguistics (Volume 1: Long Papers)*, pages 12890–12903, 2023.
- [23] Ze Liu, Yutong Lin, Yue Cao, Han Hu, Yixuan Wei, Zheng Zhang, Stephen Lin, and Baining Guo. Swin transformer: Hierarchical vision transformer using shifted windows. In *ICCV*, 2021.
- [24] Tri Dao, Dan Fu, Stefano Ermon, Atri Rudra, and Christopher Ré. Flashattention: Fast and memory-efficient exact attention with io-awareness. *Advances in neural information processing systems*, 35:16344–16359, 2022.
- [25] Tri Dao. Flashattention-2: Faster attention with better parallelism and work partitioning. *arXiv preprint arXiv:2307.08691*, 2023.
- [26] Jay Shah, Ganesh Bikshandi, Ying Zhang, Vijay Thakkar, Pradeep Ramani, and Tri Dao. Flashattention-3: Fast and accurate attention with asynchrony and low-precision. *Advances in Neural Information Processing Systems*, 37:68658–68685, 2024.
- [27] Xiaoyu Yang, Lijian Xu, Hongsheng Li, and Shaoting Zhang. One leaf reveals the season: Occlusion-based contrastive learning with semantic-aware views for efficient visual representation. In *Forty-second International Conference on Machine Learning*, 2025.
- [28] Wangyu Feng, Shawn Young, and Lijian Xu. Efficient chest x-ray representation learning via semantic-partitioned contrastive learning. *arXiv preprint arXiv:2603.7338028*, 2026.
- [29] Shawn Young, Xingyu Zeng, and Lijian Xu. Fewer tokens, greater scaling: Self-adaptive visual bases for efficient and expansive representation learning. *arXiv preprint arXiv:2511.19515*, 2026.
- [30] Xiaoyu Yang, Lijian Xu, Xingyu Zeng, Xiaosong Wang, Hongsheng Li, and Shaoting Zhang. Scalar: Spatial-concept alignment for robust vision in harsh open world. *Pattern Recognition*, 2026.
- [31] Lijian Xu, Ziyu Ni, Xinglong Liu, Xiaosong Wang, Hongsheng Li, and Shaoting Zhang. Learning a multi-task transformer via unified and customized instruction tuning for chest radiograph interpretation. *arXiv preprint arXiv:2311.01092*, 2023.
- [32] Xiaoyu Yang, Lijian Xu, Simon Yu, Qing Xia, Hongsheng Li, and Shaoting Zhang. Segmentation and vascular vectorization for coronary artery by geometry-based cascaded neural network. *IEEE Transactions on Medical Imaging*, 2024.
- [33] Xiaoyu Yang, Lijian Xu, Simon Yu, Qing Xia, Hongsheng Li, and Shaoting Zhang. Geometry-based end-to-end segmentation of coronary artery in computed tomography angiography. In *International Workshop on Trustworthy Machine Learning for Healthcare*, pages 190–196. Springer, 2023.
- [34] Zhuo Chen, Shawn Young, and Lijian Xu. Tc-ssa: Token compression via semantic slot aggregation for gigapixel pathology reasoning. *arXiv preprint arXiv:2603.01143*, 2026.
- [35] Peihang Wu and Lijian Xu. Towards efficient multimodal large language models of gigapixel pathology: A survey on token compression. *arXiv preprint*, 2026.
- [36] Lijian Xu, Hao Sun, Ziyu Ni, Hongsheng Li, and Shaoting Zhang. Medvilam: A multimodal large language model with advanced generalizability and explainability for medical data understanding and generation. *arXiv preprint arXiv:2409.19684*, 2024.

- [37] Lijian Xu, Ziyu Ni, Hao Sun, Hongsheng Li, and Shaoting Zhang. A foundation model for generalizable disease diagnosis in chest x-ray images. *arXiv preprint arXiv:2410.08861*, 2024.
- [38] Yonghan Gao, Zehong Chen, Lijian Xu, Jingzhi Chen, Jingwei Guan, and Xingyu Zeng. Zerosense: How vision matters in long context compression. *arXiv preprint arXiv:2603.7337970*, 2026.
- [39] Daniel Bolya, Cheng-Yang Fu, Xiaodong Dai, Peize Zhang, and Judy Hoffman. Token merging: Your ViT but faster. In *ICLR*, 2023.
- [40] Shixiang Tang et al. Dynamic token pruning in plain vision transformers for semantic segmentation. In *ICCV*, 2023.
- [41] Rui Zhang et al. Zero-TPrune: Zero-shot token pruning through leveraging of the attention graph. In *CVPR*, 2024.
- [42] Weidong Cao, Zeqin Feng, Fangwei Sun, Danjun Liu, Yongqiang Xie, and Zhongbo Li. A survey on visual token compression for efficient vision-language models. In *2025 5th International Conference on Advanced Algorithms and Neural Networks (AANN)*, pages 735–741. IEEE, 2025.
- [43] Jiacheng Chen et al. LLaVA-PruMerge: Adaptive token reduction for efficient large multimodal models. In *Proceedings of the IEEE/CVF International Conference on Computer Vision*, pages 22857–22867, 2025.
- [44] Haoran Zhang et al. [CLS] attention is all you need for training-free visual token pruning: Make VLM inference faster, 2024. *arXiv preprint*.
- [45] Yufei Liu et al. Divprune: Diversity-based visual token pruning for large multimodal models. In *CVPR*, 2025.
- [46] Zichen Wen, Yifeng Gao, Shaobo Wang, Junyuan Zhang, Qintong Zhang, Weijia Li, Conghui He, and Linfeng Zhang. Stop looking for “important tokens” in multimodal language models: Duplication matters more. In *Proceedings of the 2025 Conference on Empirical Methods in Natural Language Processing*, pages 9972–9991, 2025.
- [47] Ming Xu et al. Feather the throttle: Revisiting visual token pruning for vision-language model acceleration. In *ICCV*, 2025.
- [48] Yichen Li et al. Fit and prune: Fast and training-free visual token pruning for multi-modal large language models. In *AAAI*, 2025.
- [49] Zhihang Lin, Mingbao Lin, Luxi Lin, and Rongrong Ji. Boosting multimodal large language models with visual tokens withdrawal for rapid inference. In *Proceedings of the AAAI Conference on Artificial Intelligence*, volume 39, pages 5334–5342, 2025.
- [50] Qing Sun et al. Balanced token pruning: Accelerating vision language models beyond local optimization. In *NeurIPS*, 2025.
- [51] Yuan Zhang, Chun-Kai Fan, Junpeng Ma, Wenzhao Zheng, Tao Huang, Kuan Cheng, Denis Gudovskiy, Tomoyuki Okuno, Yohei Nakata, Kurt Keutzer, et al. Sparsevlm: Visual token sparsification for efficient vision-language model inference. *ICML*, 2025.
- [52] Peng Guo et al. Token pruning in multimodal large language models: Are we solving the right problem?, 2025. Findings of ACL.
- [53] Yuxin Chen et al. Flexattention for efficient high-resolution vision-language models. In *ECCV*, 2024.
- [54] Zekun Wang et al. FastVLM: Efficient vision encoding for vision language models. In *CVPR*, 2025.
- [55] Shuai Bai, Keqin Chen, Xuejing Liu, Jialin Wang, Wenbin Ge, Sibao Song, Kai Dang, Peng Wang, Shijie Wang, Jun Tang, Humen Zhong, Yuanzhi Zhu, Mingkun Yang, Zhaohai Li, Jianqiang Wan, Pengfei Wang, Wei Ding, Zheren Fu, Yiheng Xu, Jiabo Ye, Xi Zhang, Tianbao Xie, Zesen Cheng, Hang Zhang, Zhibo Yang, Haiyang Xu, and Junyang Lin. Qwen2.5-vl technical report, 2025.
- [56] Quan-Sheng Zeng, Yunheng Li, Qilong Wang, Peng-Tao Jiang, Zuxuan Wu, Ming-Ming Cheng, and Qibin Hou. A glimpse to compress: Dynamic visual token pruning for large vision-language models. *arXiv preprint arXiv:2508.01548*, 2025.
- [57] Jun Zhang, Desen Meng, Zhengming Zhang, Zhenpeng Huang, Tao Wu, and Limin Wang. p-mod: Building mixture-of-depths mllms via progressive ratio decay. In *Proceedings of the IEEE/CVF International Conference on Computer Vision*, pages 3705–3715, 2025.
- [58] Jianlin Su. Softmax hou zhuan: Xunzhao top-k de guanghua jinsi, Sep 2024.
- [59] Jia Deng, Wei Dong, Richard Socher, Li-Jia Li, Kai Li, and Li Fei-Fei. Imagenet: A large-scale hierarchical image database. In *2009 IEEE conference on computer vision and pattern recognition*, pages 248–255. IEEE, 2009.
- [60] Visual Layer. Imagenet-1k-vl-enriched, 2023. HuggingFace dataset.

- [61] Haotian Liu, Chunyuan Li, Yuheng Li, Bo Li, Yuanhan Zhang, Sheng Shen, and Yong Jae Lee. Llava-next: Improved reasoning, ocr, and world knowledge, January 2024.
- [62] Drew A Hudson and Christopher D Manning. Gqa: A new dataset for real-world visual reasoning and compositional question answering. In *Proceedings of the IEEE/CVF conference on computer vision and pattern recognition*, pages 6700–6709, 2019.
- [63] Yuan Liu, Haodong Duan, Yuanhan Zhang, Bo Li, Songyang Zhang, Wangbo Zhao, Yike Yuan, Jiaqi Wang, Conghui He, Ziwei Liu, et al. Mmbench: Is your multi-modal model an all-around player? In *European conference on computer vision*, pages 216–233. Springer, 2024.
- [64] Chaoyou Fu, Peixian Chen, Yunhang Shen, Yulei Qin, Mengdan Zhang, Xu Lin, Jinrui Yang, Xiawu Zheng, Ke Li, Xing Sun, et al. Mme: A comprehensive evaluation benchmark for multimodal large language models. *NeurIPS*, 2025.
- [65] Yifan Li, Yifan Du, Kun Zhou, Jinpeng Wang, Wayne Xin Zhao, and Ji-Rong Wen. Evaluating object hallucination in large vision-language models. In *Proceedings of the 2023 conference on empirical methods in natural language processing*, pages 292–305, 2023.
- [66] Pan Lu, Swaroop Mishra, Tanglin Xia, Liang Qiu, Kai-Wei Chang, Song-Chun Zhu, Oyvind Tafjord, Peter Clark, and Ashwin Kalyan. Learn to explain: Multimodal reasoning via thought chains for science question answering. *Advances in neural information processing systems*, 35:2507–2521, 2022.
- [67] Yash Goyal, Tejas Khot, Douglas Summers-Stay, Dhruv Batra, and Devi Parikh. Making the v in vqa matter: Elevating the role of image understanding in visual question answering. In *Proceedings of the IEEE conference on computer vision and pattern recognition*, pages 6904–6913, 2017.
- [68] Amanpreet Singh, Vivek Natarajan, Meet Shah, Yu Jiang, Xinlei Chen, Dhruv Batra, Devi Parikh, and Marcus Rohrbach. Towards vqa models that can read. In *Proceedings of the IEEE/CVF conference on computer vision and pattern recognition*, pages 8317–8326, 2019.
- [69] Bohao Li, Yuying Ge, Yixiao Ge, Guangzhi Wang, Rui Wang, Ruimao Zhang, and Ying Shan. Seed-bench: Benchmarking multimodal large language models. In *Proceedings of the IEEE/CVF Conference on Computer Vision and Pattern Recognition*, pages 13299–13308, 2024.
- [70] Jeffrey P Bigham, Chandrika Jayant, Hanjie Ji, Greg Little, Andrew Miller, Robert C Miller, Robin Miller, Aubrey Tatarowicz, Brandyn White, Samuel White, et al. Vizwiz: nearly real-time answers to visual questions. In *Proceedings of the 23rd annual ACM symposium on User interface software and technology*, pages 333–342, 2010.
- [71] Xin Zou, Di Lu, Yizhou Wang, Yibo Yan, Yuanhuiyi Lyu, Xu Zheng, Linfeng Zhang, and Xuming Hu. Don't just chase "highlighted tokens" in mllms: Revisiting visual holistic context retention. *NeurIPS*, 2025.
- [72] Kazi Hasan Ibn Arif, JinYi Yoon, Dimitrios S Nikolopoulos, Hans Vandierendonck, Deepu John, and Bo Ji. Hired: Attention-guided token dropping for efficient inference of high-resolution vision-language models. In *Proceedings of the AAAI Conference on Artificial Intelligence*, volume 39, pages 1773–1781, 2025.
- [73] Zhengyao Fang, Pengyuan Lyu, Chengquan Zhang, Guangming Lu, Jun Yu, and Wenjie Pei. Prune redundancy, preserve essence: Vision token compression in vlms via synergistic importance-diversity. In *The Fourteenth International Conference on Learning Representations*, 2025.
- [74] Long Xing, Qidong Huang, Xiaoyi Dong, Jiajie Lu, Pan Zhang, Yuhang Zang, Yuhang Cao, Conghui He, Jiaqi Wang, Feng Wu, et al. Pyramidrop: Accelerating your large vision-language models via pyramid visual redundancy reduction. *CVPR*, 2025.